Society of Medical Education & Research

2024, Volume 4, Issue 1, Page No: 47-66
ISSN: 3108-4834

Archive of International Journal of Cancer and Allied Science

An m6A-Modified Circular RNA-Encoded Oncoprotein Drives a Positive Feedback Loop Promoting Colorectal Cancer Liver Metastasis

Junpei Hiroshi Tanaka[1]*, Kenta Masaru Fujimoto[1]

[1]Division of Clinical Oncology, Kobe University Graduate School of Medicine, Kobe, Japan.

***E-mail** ✉ j.tanaka.kobe@outlook.com

Abstract

Colorectal cancer (CRC) frequently metastasizes to the liver, which is the main driver of patient mortality. While circular RNAs (circRNAs) have emerged as critical regulators in cancer, their role in promoting CRC liver metastasis is still poorly understood. We examined circ-YAP expression using qRT-PCR and in situ hybridization, and assessed its impact on CRC cell proliferation, migration, and invasion through CCK-8, wound healing, and transwell assays. Mechanistic studies were performed using RNA immunoprecipitation, pull-down, luciferase reporter, and chromatin immunoprecipitation assays. The functional relevance of circ-YAP in liver metastasis was evaluated in a patient-derived xenograft (PDX) mouse model. Circ-YAP was markedly elevated in CRC tissues with liver metastasis and predicted worse clinical outcomes. Functionally, circ-YAP enhanced CRC cell motility in vitro and promoted hepatic colonization in vivo. Mechanistically, circ-YAP encodes a truncated 220-amino acid protein, YAP-220aa, which competes with LATS1, leading to YAP activation via dephosphorylation and nuclear translocation, thereby upregulating metastasis-related genes. Translation of circ-YAP is facilitated by m6A modification, mediated by YTHDF3 and the eIF4G2 initiation complex. Remarkably, circ-YAP transcription is reinforced by the YAP/TEAD complex, forming a self-amplifying positive feedback loop. Our study uncovers a novel circRNA-encoded oncoprotein that drives CRC liver metastasis and highlights circ-YAP as a potential prognostic biomarker and therapeutic target.

Keywords: Circular RNA, m6A, Translation, Hippo pathway, Colorectal cancer metastasis

Introduction

Colorectal cancer (CRC) ranks among the most prevalent malignancies of the digestive tract, with its incidence and mortality standing third and second, respectively, among all cancers [1]. Tumor metastasis is the primary cause of CRC-related deaths. Clinically, 45–60% of CRC patients develop liver metastases, and over 90% of these lesions are initially unresectable [2]. Without surgical intervention, the median survival of patients with liver metastases is only 6.9 months, with a 5-year survival rate below 5% [3]. Therefore, elucidating the mechanisms driving CRC liver metastasis and identifying new therapeutic targets are critical for improving patient outcomes.

Circular RNAs (circRNAs) are a distinct class of endogenous RNAs characterized by covalently closed loop structures, lacking the conventional 5′ cap and 3′ polyadenylated tail [4]. They are generated through spliceosome-mediated back-splicing, allowing a single genetic locus to produce multiple circRNA isoforms [5]. High-throughput sequencing and computational analyses have revealed that circRNAs are highly conserved and exhibit tissue-, cell-, or disease-specific expression patterns [6]. Increasing evidence implicates circRNAs in various human diseases, with some serving as potential biomarkers for disease progression and prognosis [7, 8]. Functionally, circRNAs exert diverse regulatory roles. Many act as “miRNA sponges,” exemplified by CDR1as, which harbors over 70 miR-7 binding sites [9, 10]. Others directly interact with proteins, serving as scaffolds or

Access this article online https://smerpub.com/

Received: 24 October 2023; **Accepted:** 16 January 2024

How to cite this article: Tanaka JH, Fujimoto KM. An m6A-Modified Circular RNA-Encoded Oncoprotein Drives a Positive Feedback Loop Promoting Colorectal Cancer Liver Metastasis. Arch Int J Cancer Allied Sci. 2024;4(1):47-66. https://doi.org/10.51847/75drJfVhEu

decoys to modulate gene expression [11]. Notably, recent studies indicate that some circRNAs can be translated into functional peptides. For instance, circ-Nlgn encodes Nlgn-173aa, a novel transcription factor implicated in myocardial fibrosis [12], while circRNA-derived truncated proteins such as E-Cad-254aa and ARHGAP35-1289aa play critical roles in glioma [13] and hepatocellular carcinoma [14], respectively. Due to their covalently closed structure, circRNAs enable cap-independent translation, which can be mediated by internal ribosome entry sites (IRES) or N6-methyladenosine (m6A) modification [15].

m6A is the most abundant internal RNA modification in eukaryotes, dynamically regulated by "writers" (METTL3/14, WTAP), "erasers" (FTO, ALKBH5), and "readers" (YTHDF1/2/3, YTHDC1/2) [16]. Despite these insights, only a small fraction of circRNA-encoded proteins has been functionally characterized, leaving the majority unexplored.

In this study, we identified circ-YAP as a key driver of CRC liver metastasis. Circ-YAP harbors a 220-amino acid open reading frame (ORF) and encodes a novel YAP isoform, YAP-220aa, in an m6A-dependent manner. Mechanistically, YAP-220aa activates YAP signaling by inhibiting LATS1-mediated YAP phosphorylation and cytoplasmic sequestration.

Materials and Methods

Clinical specimens and cell culture

CRC tissue specimens were collected from Sun Yat-sen University Cancer Center, encompassing both fresh-frozen samples (30 normal, 23 CRC, 17 CRC with liver metastasis, 9 CRC with lung metastasis, and 7 CRC with brain metastasis) and paraffin-embedded samples (25 normal, 211 CRC, and 56 CRC with liver metastasis). All participants provided written informed consent, and the study protocol was approved by the Institutional Review Board of Sun Yat-sen University Cancer Center (SL-B2022-276-02).

Normal colonic epithelial FHC cells (CRL-1831) and CRC cell lines—HT-29 (HTB-38), SW480 (CCL-228), DLD1 (CCL-221), HCT116 (CCL-247), SW620 (CCL-227), and LoVo (CCL-229)—were obtained from ATCC and cultured in DMEM supplemented with 10% fetal bovine serum (FBS). Patient-derived xenograft (PDX) TC71 cells (XENTECH, No. XTM-233_CXT-399/R5700) were maintained in advanced DMEM/F12 medium with 8% FBS, 1% glutamine, and 1% antibiotics. All cell cultures were routinely screened for mycoplasma contamination.

RNA extraction and quantitative real-time PCR

Total RNA was extracted using Trizol reagent (Invitrogen) and reverse-transcribed into cDNA (1 μg RNA per reaction) using PrimeScript RT Enzyme (Takara Bio). Quantification was carried out using TB Green Premix Ex Taq II (Takara Bio), with primer specificity validated via melt-curve analysis.

FISH, ISH, and IHC assays

For FISH, a FAM-labeled probe targeting the circ-YAP back-splice junction was designed by GenePharma (Shanghai, China) and hybridized following the manufacturer's protocol. ISH on paraffin-embedded tissues was performed by proteinase K digestion, overnight hybridization with a 5'-digoxin-labeled circ-YAP probe at 55 °C, followed by incubation with anti-digoxin antibody (Roche) at 4 °C. Signal detection was performed using NBT/BCIP substrate.

For IHC, tissue sections were probed with antibodies against YAP-220aa (GenScript) at 1:50 and YAP (#14,074, CST) at 1:400, followed by visualization using DAB. Staining intensity and distribution were evaluated using the H-score method as previously described [17].

Vectors, oligonucleotides, and transfection

To silence circ-YAP, the CRISPR/Cas13d system was employed [18]. Three single-guide RNAs (sgRNAs) targeting the circ-YAP back-splice junction (gRNA#1: TCCTTTCCTTAACAGGCCAGTACTGATGCA; gRNA#2: TCAGATCCTTTCCTTAACAGGCCAGTACTG; gRNA#3: TCCTTAACAGGCCAGTACTGATGCAGGCAC) were designed, synthesized, and cloned into the pLKO.1 vector carrying RfxCas13d direct repeats. Lentiviral particles were generated using psPAX2 and pMD2.G plasmids and used to infect CRC cells in the presence of 5 μg/mL polybrene, followed by puromycin selection (1.5 μg/mL).

For circ-YAP overexpression, the full-length circRNA was synthesized and inserted into the pLV-circ-Puro vector containing flanking reverse complementary sequences. YTHDF3 knockout was achieved by inserting three sgRNAs targeting YTHDF3 (gRNA#1: CTAAGCGAATATGCCGTAAT; gRNA#2: GTGGACTATAATGCGTATGC; gRNA#3:

AAAGTTGACTCTTCTCGTAA) into a CRISPR/Cas9 All-in-One lentiviral vector, followed by single-clone selection. shRNA-mediated YAP knockdown (sh-YAP targeting 3′-UTR: CCCAGTTAAATGTTCACCAAT) was conducted using the pLKO.1 vector. Additionally, siRNAs targeting eIF4G2 and TEAD transcription factors were purchased from Ribobio (Guangzhou, China). Plasmids encoding YAP-5SA and YAP-5SA/S94A were obtained from Addgene. m6A motif mutations were generated using the Q5 Site-Directed Mutagenesis Kit (New England Biolabs) according to manufacturer instructions. All constructs were validated by Sanger sequencing. Transfections were performed using Lipofectamine 3000 (Invitrogen), and efficiency was confirmed via qRT-PCR or western blotting.

Wound healing, transwell migration, and proliferation assays

Cell migratory capacity was assessed using wound healing assays. CRC cells were cultured in 6-well plates, and a linear scratch was made using a sterile pipette tip. Cells were then maintained in serum-free DMEM for 24 h, and migration distance was measured. For invasion assays, cells were seeded in the upper chamber of 8 μm pore-size transwell inserts (BD Falcon, CA, USA), while the lower chamber contained 600 μL complete medium. After 24 h, invaded cells were fixed and stained with crystal violet. Cell proliferation was determined using the CCK-8 assay (Dojindo, Kumamoto, Japan); 10 μL of reagent was added per well in 96-well plates, incubated at 37 °C for 2 h, and absorbance at 450 nm was recorded.

CRC liver metastasis models

For the spontaneous liver metastasis model, TC71 PDX cells with or without circ-YAP knockdown were trypsinized, washed in cold PBS, and 3 × 10^6 cells in 50 μL were orthotopically injected into the colonic subserosa of NOD/SCID mice. After 10 weeks, mice were euthanized and livers were examined for metastatic lesions. In the experimental metastasis model, 1 × 10^6 TC71 PDX cells in 20 μL PBS were injected into the spleen, and liver metastases were quantified after 4 weeks. Metastatic burden was calculated as the product of nodule number and diameter. All animal procedures were approved by the Institutional Animal Care and Use Committee of Sun Yat-sen University (SYSU-IACUC-2021-000653).

Western blotting and co-immunoprecipitation (Co-IP)

Cells were washed with ice-cold PBS and lysed in RIPA buffer supplemented with a protease inhibitor cocktail (Roche). Protein concentrations were determined using the Pierce™ BCA Protein Assay Kit (Invitrogen). Equal amounts of protein were resolved on 8–10% SDS-PAGE gels and transferred onto PVDF membranes. Membranes were incubated with appropriate primary and secondary antibodies, and protein bands were visualized using Pierce™ ECL Western Blotting Substrate (Invitrogen).

For Co-IP assays, lysates were pre-cleared with 20 μL protein A/G agarose beads (Gibco) and then incubated with the indicated primary antibodies at 4 °C for 3 h. Protein complexes were captured by incubation with 40 μL protein A/G agarose for 30 min at 4 °C, eluted, and analyzed by SDS-PAGE followed by western blotting. Primary antibodies included: anti-Flag, anti-YAP-220aa, anti-METTL3, anti-YTHDF1/2/3, anti-eIF4G2, anti-eIF4A/B, anti-LATS1, anti-YAP, anti-14-3-3, p-YAP (S127), anti-TEAD1, anti-Tubulin, anti-CDX2, anti-GAPDH, and anti-Histone H3

Immunofluorescence (IF)

CRC cells were fixed with 4% paraformaldehyde, permeabilized using 0.1% Triton X-100, and blocked with 5% BSA for 30 min at room temperature. Cells were incubated overnight at 4 °C with antibodies against Flag, YAP-220aa, or YAP, followed by 1 h incubation with fluorescently labeled secondary antibodies. Nuclei were counterstained with DAPI, and fluorescence signals were captured using a fluorescence microscope.

RNA immunoprecipitation (RIP) and methylated RNA immunoprecipitation (meRIP)

RIP was performed using the Magna RIP Kit (Millipore) following the manufacturer's protocol. Briefly, CRC cell lysates were incubated with magnetic beads pre-coated with anti-YTHDF3 or control IgG at 4 °C for 12 h. RNA-protein complexes were digested with proteinase K, and the enriched RNA was extracted with Trizol and analyzed by qRT-PCR.

For meRIP, total RNA was fragmented to ≤100 nt at 70 °C for 5 min and incubated with anti-m6A antibody (Millipore) and Protein A/G magnetic beads overnight at 4 °C. m6A-enriched RNA was eluted with 5′-monophosphate sodium salt, purified, and quantified by qRT-PCR.

RNA pull-down assays

For in vivo pull-down, a biotin-labeled circ-YAP junction probe was incubated with CRC cell lysates for 5 h at 4 °C, followed by capture with streptavidin magnetic beads for 1 h. Bound proteins were eluted and analyzed by western blot.

For in vitro assays, linear circ-YAP was transcribed using the T7 Transcription Kit (Invitrogen), biotin-labeled (Roche), and circularized using T4 RNA ligase I. Biotinylated circ-YAP was incubated with recombinant human YTHDF3 protein (Abcam) in binding buffer (20 mM Tris, 150 mM NaCl, 1% Triton X-100, 2 mM DTT, 1 mM EDTA) at 4 °C for 1 h. Complexes were captured with streptavidin beads and analyzed by western blot.

Detection of nascent circ-YAP transcripts

Transcription was blocked using 5,6-dichlorobenzimidazole 1-β-D-ribofuranoside (DRB; Sigma). Following DRB release, newly synthesized RNA was labeled with 4-thiouridine (4sU; Sigma). Total RNA was extracted, biotinylated, and pulled down using streptavidin beads. Enriched nascent RNA was washed and quantified by qRT-PCR to assess circ-YAP transcriptional dynamics.

Luciferase reporter assays

To assess YAP transcriptional activity, CRC cells with circ-YAP knockdown or overexpression were transfected with the 8xGTIIC-luciferase reporter plasmid (#34,615, Promega) using Lipofectamine 3000 (Invitrogen). After 48 h, luciferase activity was measured using the Dual-Luciferase Reporter Assay System (Promega) according to the manufacturer's instructions. For evaluation of circ-YAP promoter activity, full-length or truncated promoter fragments were cloned into the pGL3-basic vector (Promega) and co-transfected with pRL-TK and YAP-5SA plasmids. Relative luciferase signals were quantified as described above. All experiments were performed in triplicate using 48-well plates.

Chromatin immunoprecipitation (ChIP) and re-ChIP

ChIP assays were performed using the SimpleChIP® Plus Sonication Chromatin IP Kit (#56,383, CST). Antibodies used included anti-YAP (#14,074, CST), anti-RNA polymerase II (Pol II, N-20, Santa Cruz), and anti-phospho-Pol II (S5, ab5408, Abcam). For sequential ChIP (re-ChIP), DNA-protein complexes immunoprecipitated with anti-YAP were eluted, treated with 10 mM DTT at 37 °C for 30 min, and then re-immunoprecipitated using anti-TEAD1 (#610,922, BD Biosciences). The final DNA was analyzed by qPCR.

DNA pull-down assay

Biotinylated probes targeting the circ-YAP promoter were incubated with sonicated nuclear extracts overnight at 4 °C. Streptavidin magnetic beads (Invitrogen) were added and incubated for 1 h at 4 °C. After three washes, bound proteins were eluted with 1× loading buffer and analyzed by western blot for YAP and TEAD1 enrichment.

Statistical analysis

Data are presented as mean ± standard deviation (SD). Comparisons between two groups were performed using two-tailed Student's t-test. Receiver operating characteristic (ROC) curves were used to evaluate predictive performance. Kaplan–Meier survival curves were generated and analyzed using the log-rank test. Statistical analyses and graphs were performed using GraphPad Prism 7 (La Jolla, CA, USA). P-values <0.05 were considered statistically significant.

Results and Discussion

Circ-YAP is associated with CRC liver metastasis

To identify circRNAs with potential translational activity in CRC liver metastasis, circRNA microarray and ribosome-associated RNA sequencing data were analyzed. Circ-YAP was among the circRNAs upregulated in liver metastatic CRC and predicted to have translation potential. Gene set enrichment analysis (GSEA) revealed that circ-YAP expression correlated with a liver-specific gene signature.

Expression analysis in fresh-frozen tissues showed that circ-YAP was modestly elevated in primary CRC compared with normal tissue, but significantly overexpressed in CRC with liver metastases **(Figure 1a)**. No significant differences were observed in lung or brain metastases. Similarly, high circ-YAP levels were observed in CRC cell lines with strong metastatic potential **(Figure 1b)**.

Sequence analysis indicated that circ-YAP originates from back-splicing between exons 2 and 7 of YAP pre-mRNA, resulting in an 842-bp circular transcript **(Figure 1c)**. Circ-YAP, unlike its linear counterpart, was resistant to RNase R treatment **(Figure 1d)** and displayed a half-life exceeding 24 h **(Figure 1e)**. qRT-PCR and FISH assays demonstrated predominant cytoplasmic localization of circ-YAP **(Figure 1f)**.

In paraffin-embedded tissues, ISH analysis confirmed significant upregulation of circ-YAP in CRC with liver metastasis **(Figures 1g–1h)**, achieving an area under the curve (AUC) of 0.8433 (95% CI: 0.7645–0.9220); **(Figure 1i)**. Clinically, higher circ-YAP expression was associated with shorter overall survival **(Figure 1j)**. Circ-YAP levels remained stable under varying pH and repeated freeze-thaw cycles.

Collectively, these data confirm that circ-YAP is a bona fide circRNA and suggest its potential as a prognostic biomarker for CRC liver metastasis.

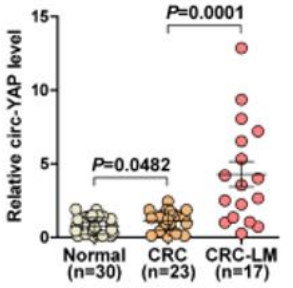

a)

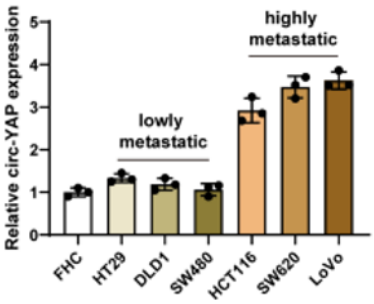

b)

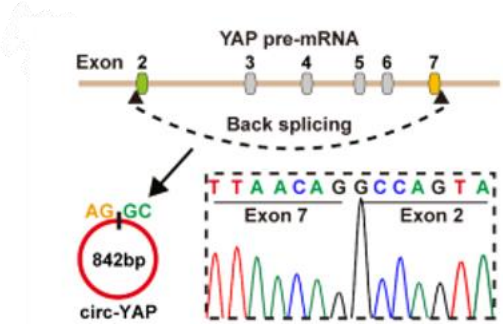

c)

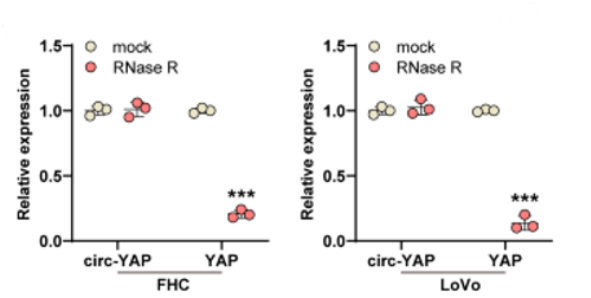

d)

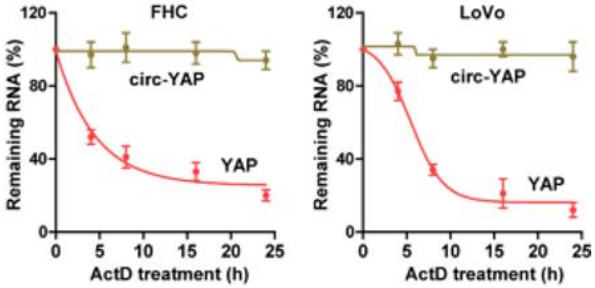

e)

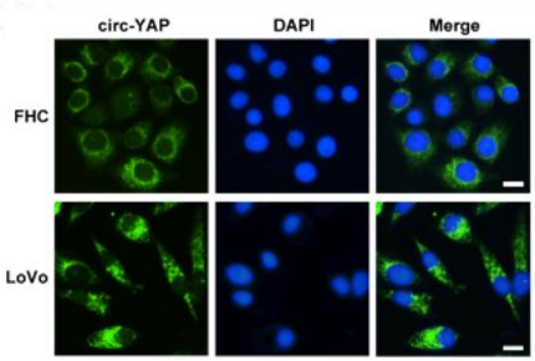

f)

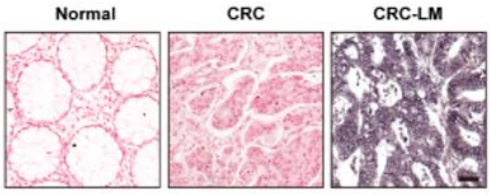

g)

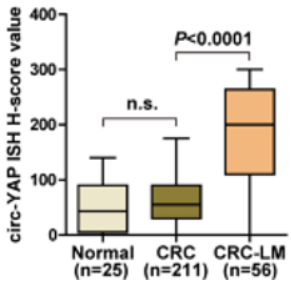

h)

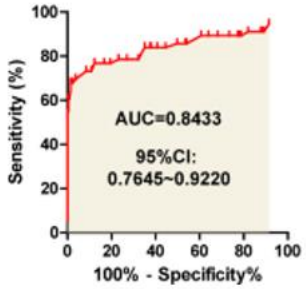

i)

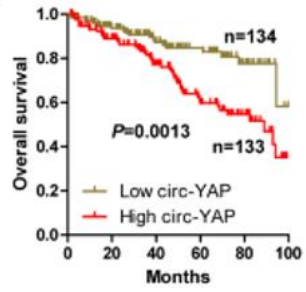

j)

Figure 1. Identification of circ-YAP in CRC liver metastasis tissues.

(a, b) qRT-PCR analysis of circ-YAP expression in CRC patient tissues and various CRC cell lines. (c) Sanger sequencing confirming the back-splice junction of circ-YAP. (d, e) Resistance of circ-YAP to 3 U/μg RNase R treatment and stability under 5 μg/mL Actinomycin D treatment, analyzed by qRT-PCR, compared with linear YAP mRNA. (f) FISH assay showing subcellular localization of circ-YAP; nuclei were stained with DAPI. Scale bar: 25 μm. (g, h) ISH staining of circ-YAP in paraffin-embedded CRC tissues; dark purple signals indicate positive staining. Scale bar: 50 μm. (i) ROC curve analysis assessing the predictive value of circ-YAP expression for CRC liver metastasis. (j) Kaplan–Meier survival analysis comparing patients with high versus low circ-YAP expression. ***P < 0.001. Data in panels B, D, and E represent mean ± SD of three independent experiments performed in triplicate.

Knockdown of circ-YAP reduces CRC liver metastasis

To determine the functional role of circ-YAP, CRISPR/Cas13d-mediated knockdown was performed. All three designed sgRNAs effectively reduced circ-YAP levels without altering linear YAP mRNA expression **(Figure 2a)**. Functional assays demonstrated that circ-YAP silencing significantly impaired LoVo cell migration, as shown by wound healing and transwell assays **(Figures 2b–2e)**. Similar inhibitory effects were observed in SW620 cells.

Conversely, overexpression of circ-YAP in CRC cell lines with low endogenous levels enhanced both migratory and invasive capacities **(Figures 2f–2h)**. Notably, circ-YAP manipulation did not impact cell proliferation, as measured by CCK-8 assay.

In vivo, a spontaneous CRC liver metastasis model was established by orthotopic injection of TC71 PDX cells into the colon wall of NOD/SCID mice **(Figure 2i).** After 10 weeks, 50% of control mice developed liver metastases, whereas only 6.7% of mice with circ-YAP knockdown showed metastatic lesions **(Figures 2j and 2k)**. In an experimental liver metastasis model via intrasplenic injection of TC71 cells, circ-YAP depletion significantly reduced metastatic burden. IHC staining for CDX2 confirmed that the metastatic lesions were derived from CRC cells rather than hepatocytes or immune cells. These findings collectively demonstrate that circ-YAP is a key regulator of CRC cell invasiveness and liver metastasis.

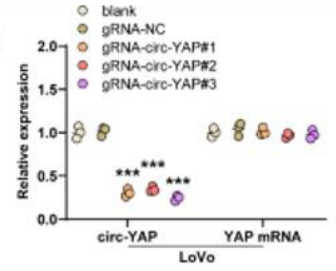

a)

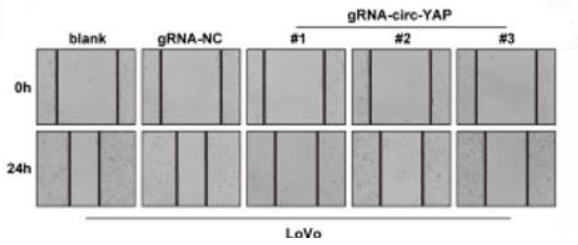

b)

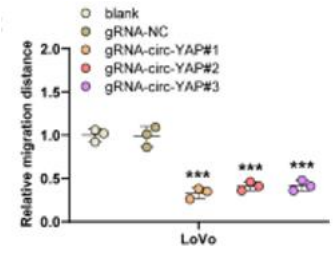

c)

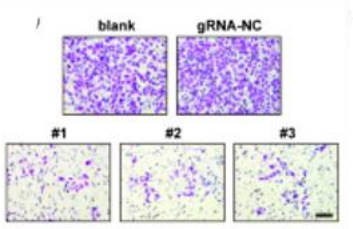

d)

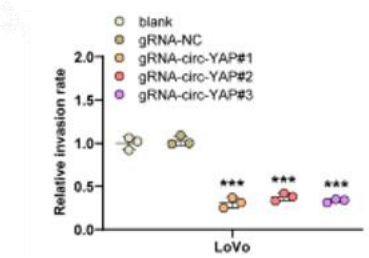

e)

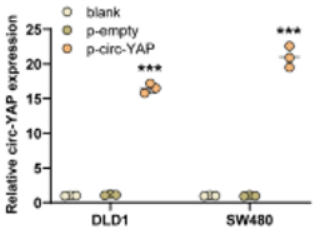

f)

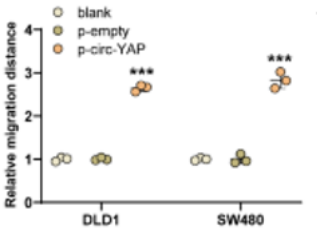

g)

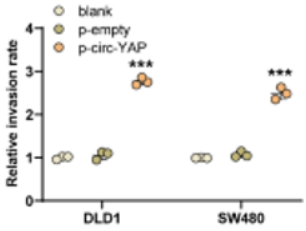

h)

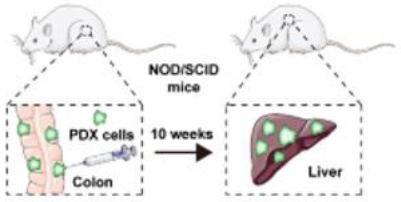

i)

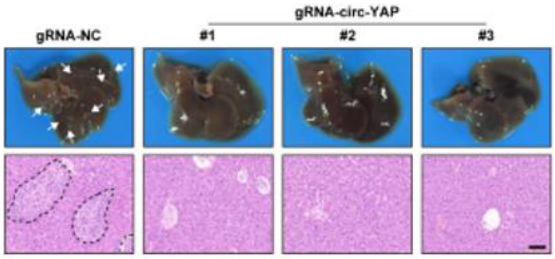

j)

CRC liver metastasis incidence

Parameter	gRNA-NC	gRNA-circ-YAP		
		#1	#2	#3
Number	5/10	1/10	0/10	1/10
Percentage	50%	10%	0%	10%

k)

Figure 2. Silencing circ-YAP reduces CRC liver metastasis burden.

(a) qRT-PCR analysis confirming the efficiency of circ-YAP knockdown using three different sgRNAs. (b, c) Wound healing assays assessing migratory capacity of LoVo cells after circ-YAP silencing. (d, e) Transwell invasion assays of CRC cells with circ-YAP knockdown. Scale bar: 100 μm. (f) qRT-PCR confirming circ-YAP overexpression. (g, h) Migration and invasion assays in DLD1 and SW480 cells following circ-YAP overexpression. (i) Schematic illustration of the spontaneous CRC liver metastasis model. (j) Representative images of liver metastases in control and circ-YAP-silenced groups. Scale bar: 100 μm. (k) Incidence of liver metastasis in each group. ***$P < 0.001$. Data in panels a, c, e, f, g, and h represent mean ± SD from three independent experiments performed in triplicate.

Circ-YAP encodes a novel YAP protein isoform, YAP-220aa

Sequence analysis revealed that circ-YAP contains an open reading frame (ORF) spanning the back-splice junction, encoding a putative 220-amino acid protein

(Figures 3a and 3b). To test its translational potential, a Flag tag was incorporated into the circ-YAP overexpression construct by splitting the tag sequence across the junction site adjacent to the stop codon **(Figure 3c).** Transfection into HEK293T cells produced a ~26 kDa protein detected by anti-Flag antibody **(Figure 3d)**. Enhanced protein expression was confirmed by Coomassie staining, and mass spectrometry verified the unique amino acid sequence of YAP-220aa **(Figure 3e)**. A rabbit polyclonal antibody against YAP-220aa was generated and validated for detection of the endogenous protein **(Figure 3f)**. Because circRNA translation can be driven by internal ribosome entry sites (IRES) or N6-methyladenosine (m6A) modification, two candidate IRES sequences were tested using a dual-luciferase system (Figure S3A), but no significant activity was observed compared to control, indicating IRES-independent translation. Notably, a conserved m6A motif ("GGACA") near the start codon was identified **(Figure 3b)**. Mutation of adenine to cytosine abolished YAP-220aa expression **(Figure 3d)**, confirming the essential role of m6A in circ-YAP translation.

Subcellular localization analysis showed predominant cytoplasmic distribution of YAP-220aa **(Figure 3g)**, with higher expression in highly metastatic CRC cell lines **(Figure 3h)**. Silencing METTL3, the m6A methyltransferase, significantly reduced endogenous YAP-220aa levels **(Figure 3i)**, and circ-YAP was more heavily m6A-modified in highly metastatic cells **(Figure 3j)**. Functionally, overexpression of wild-type circ-YAP enhanced migration and invasion of HT29 and SW480 cells, whereas the m6A-mutant construct failed to do so **(Figures 3k and 3l).**

These results demonstrate that circ-YAP exerts its pro-metastatic function by translating into a novel YAP protein isoform, YAP-220aa, in an m6A-dependent manner.

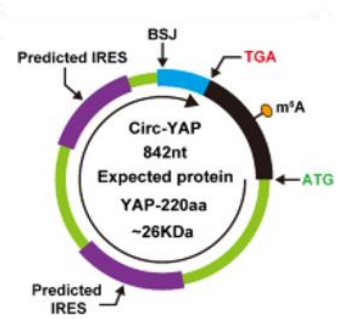

a)

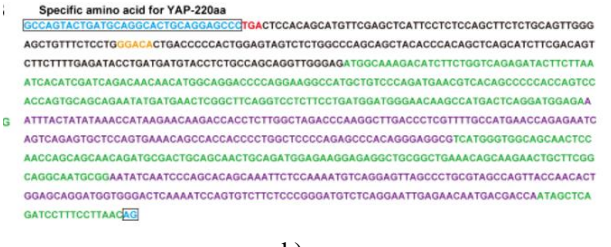

b)

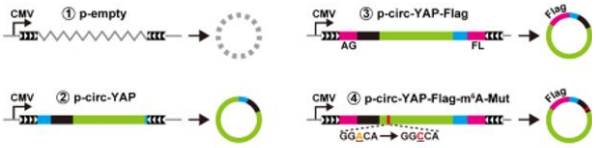

c)

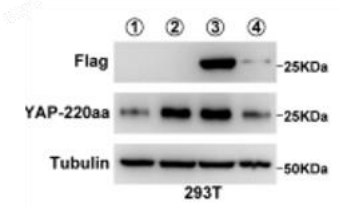

d)

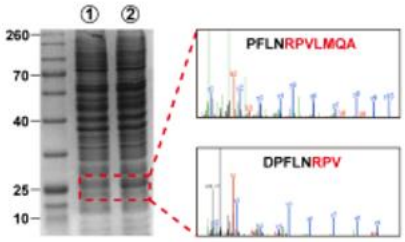

e)

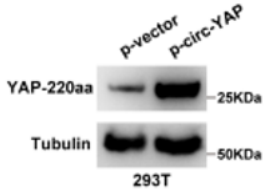

f)

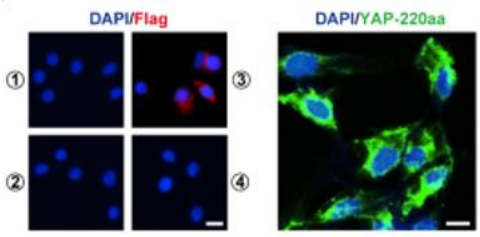

g)

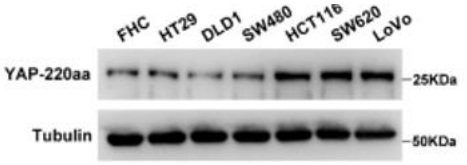

h)

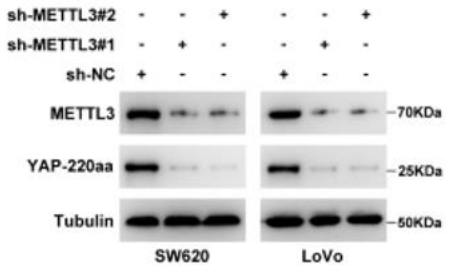

i)

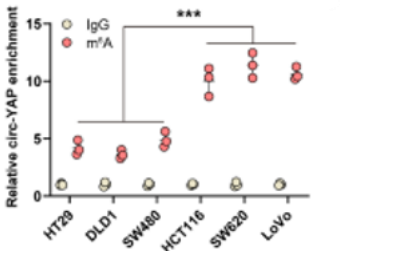

j)

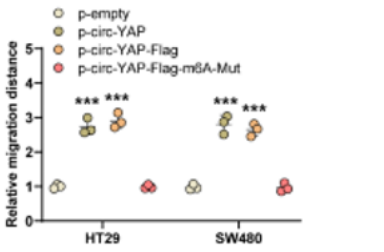

k)

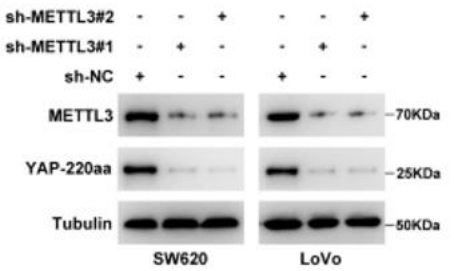

i)

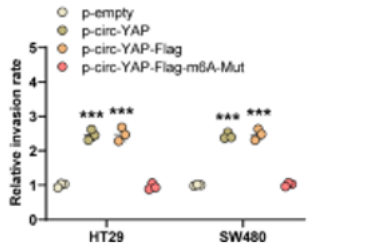

l)

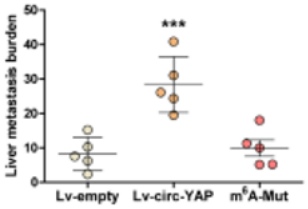

m)

Figure 3. Circ-YAP encodes YAP-220aa in an m6A-dependent manner**.**

(a, b) Schematic representation and full-length sequence of circ-YAP. (c) Diagram illustrating the construction of circ-YAP and Flag-tagged vectors. (d) Western blot showing Flag and YAP-220aa protein expression in HEK293T cells transfected with the indicated constructs. (e) Coomassie blue staining of proteins from control and circ-YAP-overexpressing cells, with subsequent mass spectrometry analysis confirming YAP-220aa sequence. (f) Western blot detecting endogenous YAP-220aa in circ-YAP-overexpressing cells. (g) Immunofluorescence staining for Flag and YAP-220aa in HEK293T cells. Scale bar: 25 μm. (h) Western blot analysis of YAP-220aa across CRC cell lines. (i) Effect of METTL3 knockdown on YAP-220aa protein levels. (j) meRIP assay showing m6A modification on circ-YAP in CRC cells. (k, l) Migration and invasion assays in HT29 and SW480 cells following transfection with wild-type or m6A-mutant circ-YAP constructs. (m) Experimental liver metastasis model testing the effect of wild-type or m6A-mutant circ-YAP on metastatic burden (n = 5 per group). ***P < 0.001. Data in panels j–l represent mean ± SD of three independent experiments performed in triplicate. Uncropped western blots are provided in the Original Blot Image file.

m6A reader YTHDF3 is essential for circ-YAP translation

To identify which m6A reader facilitates circ-YAP translation, we examined YTHDF1, YTHDF2, and YTHDF3. Knockdown of YTHDF3, but not YTHDF1 or YTHDF2, markedly inhibited the increase in YAP-220aa protein induced by circ-YAP overexpression **(Figure 4a).** Circ-YAP transcript levels remained unaffected by depletion of any YTHDF protein.

To further validate this, YTHDF3 knockout CRC cell lines were generated using CRISPR/Cas9. In these YTHDF3−/− LoVo and SW620 cells, Flag-tagged circ-

YAP translation was abolished **(Figures 4b and 5c)**. Conversely, overexpression of wild-type YTHDF3 enhanced YAP-220aa levels, an effect lost upon deletion of the functional YTH domain **(Figure 4d)**. RIP and RNA pull-down assays confirmed the physical interaction between circ-YAP and YTHDF3 **(Figures 4e and 4f)**. Moreover, in vitro synthesized circ-YAP directly bound to recombinant GST-YTHDF3 protein **(Figure 4g)**.

Since the non-canonical translation initiation factor eIF4G2 is required for YTHDF3-mediated translation [19], Co-IP assays demonstrated that YTHDF3 forms an endogenous complex with eIF4G2 in both SW620 and LoVo cells **(Figure 4h)**. Silencing eIF4G2 significantly reduced YAP-220aa protein expression **(Figure 4i)**. RNA pull-down experiments revealed enrichment of eIF4G2 and eIF4A/B by circ-YAP, which was abolished in YTHDF3 knockout cells **(Figures 4j and 4k)**, indicating that circ-YAP recruits the eIF4G2 translation initiation complex via YTHDF3.

Functionally, circ-YAP-induced enhancement of CRC cell invasion was significantly attenuated upon YTHDF3 knockout or eIF4G2 silencing **(Figures 4l and 4m).**

These findings demonstrate that YTHDF3 acts as a critical m6A reader, mediating circ-YAP translation and promoting its pro-metastatic effects through recruitment of the eIF4G2 translational machinery.

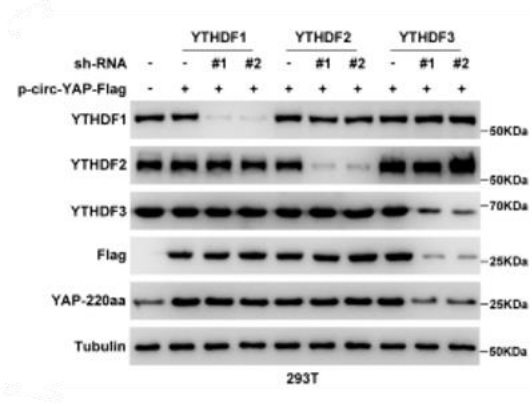

a)

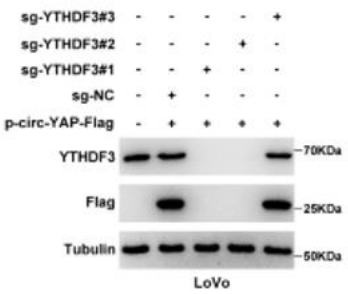

b)

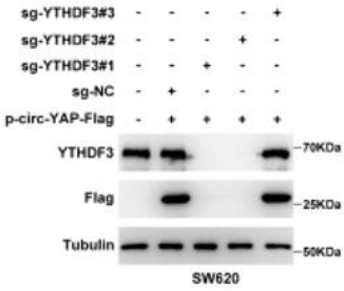

c)

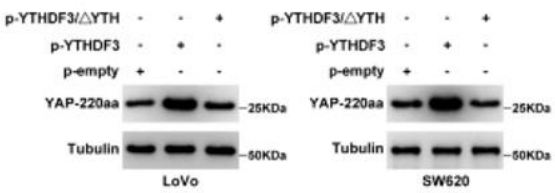

d)

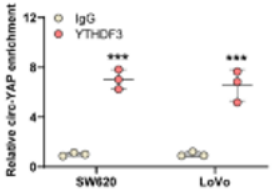

e)

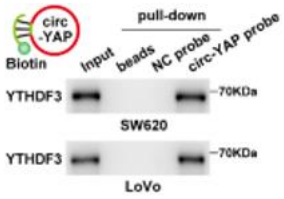

f)

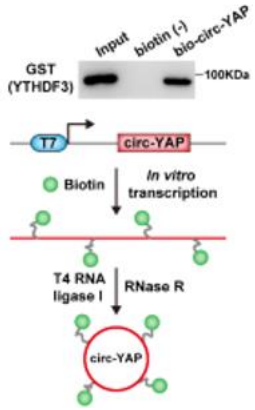

g)

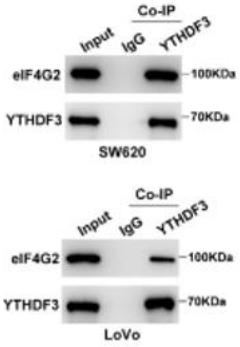

h)

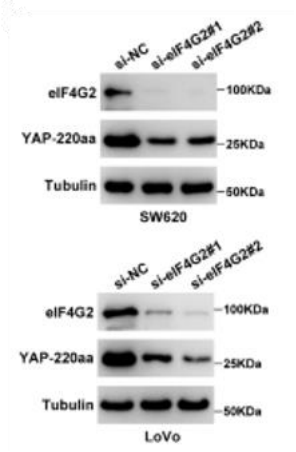

i)

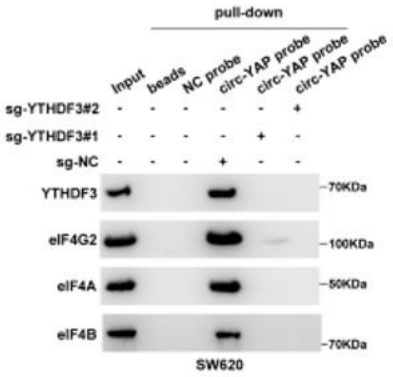

j)

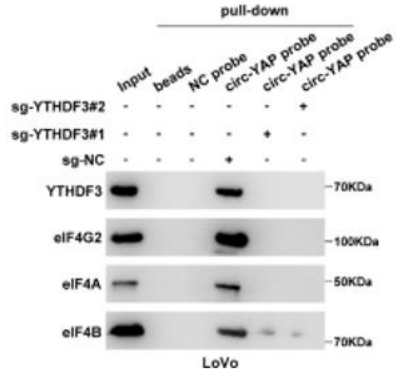

k)

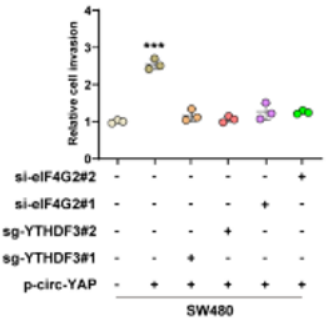

l)

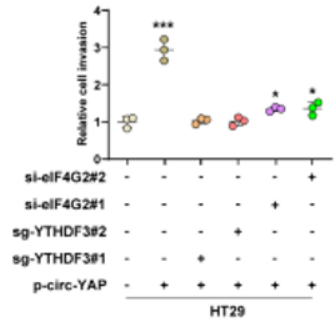

m)

Figure 4. YTHDF3 facilitates circ-YAP translation by recruiting the eIF4G2 initiation complex.

(a) Western blot showing the effect of depleting YTHDF1, YTHDF2, or YTHDF3 on YAP-220aa expression in 293T cells overexpressing circ-YAP. (b, c) Loss of YTHDF3 prevents production of YAP-220aa in LoVo and SW620 cells. (d) Overexpression of YTHDF3 enhances YAP-220aa, whereas deletion of its active YTH domain abrogates this effect. (e) RIP assays confirm that circ-YAP associates with YTHDF3. (f, g) Biotin-labeled circ-YAP pull-down experiments demonstrate YTHDF3 binding both in vitro and in cell lysates. (h) Co-immunoprecipitation shows YTHDF3 physically interacts with eIF4G2. (I) Knockdown of eIF4G2 reduces YAP-220aa protein levels. (J, K) RNA pull-down assays reveal circ-YAP recruits eIF4G2 and eIF4A/B in a YTHDF3-dependent manner. (l, m) Loss of YTHDF3 or eIF4G2 impairs circ-YAP-driven cell invasion in SW480 and HT29 cells. Data represent mean ± SD from three independent experiments. *P < 0.05; ***P < 0.001.

YAP-220aa binds LATS1 and facilitates YAP nuclear accumulation

Analysis of the YAP-220aa amino acid sequence revealed that it contains the WW1/2 domain of YAP, a motif essential for LATS1 interaction and subsequent YAP phosphorylation, which leads to 14-3-3–mediated cytoplasmic sequestration [20]. Based on this observation, we hypothesized that YAP-220aa could competitively associate with LATS1, thereby preventing YAP phosphorylation. Consistent with this hypothesis, LATS1 was efficiently pulled down by a Flag antibody in HEK293T cells expressing the p-circ-YAP-Flag construct; notably, this interaction was lost upon deletion of the WW1/2 domain **(Figure 5a)**. In addition, endogenous interactions between YAP-220aa and LATS1 were detected in LoVo and SW620 cells **(Figures 5b and 5c)**. Silencing circ-YAP significantly enhanced the binding of YAP to LATS1 and 14-3-3 **(Figures 5d and 5e).**

Furthermore, circ-YAP depletion led to reduced YAP-220aa levels and elevated YAP phosphorylation in CRC cells, effects that were reversed by overexpression of wild-type circ-YAP but not by an m6A-mutant form **(Figures 5f and 5g)**. In line with these findings, ectopic expression of circ-YAP promoted YAP translocation from the cytoplasm to the nucleus, whereas this effect was abolished following m6A mutation **(Figures 5h and 5i)**. Correspondingly, YAP reporter activity and the expression of downstream metastasis-associated genes were markedly decreased upon circ-YAP knockdown **(Figures 5j and 5k)**, while overexpression of wild-type circ-YAP, but not the m6A-deficient variant, produced the opposite effects.

Functionally, circ-YAP-induced enhancement of cell migration, invasion, and liver metastatic burden was significantly suppressed by YAP silencing or treatment with verteporfin, a YAP inhibitor **(Figures 5l–5n)**. Collectively, these results demonstrate that circ-YAP-derived YAP-220aa drives CRC progression and liver metastasis by activating YAP signaling through direct interaction with LATS1.

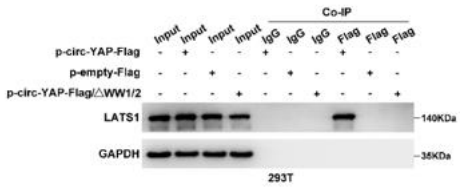

a)

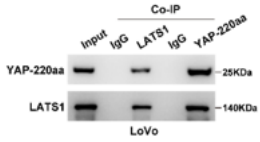

b)

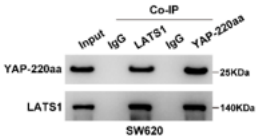

c)

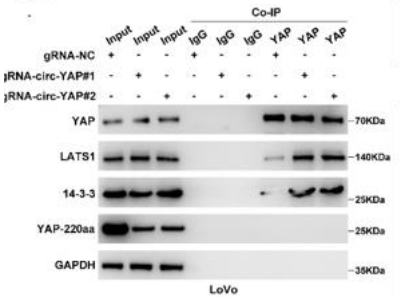

d)

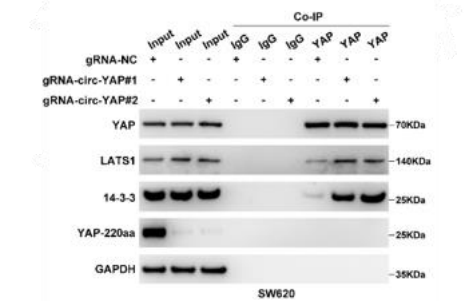

e)

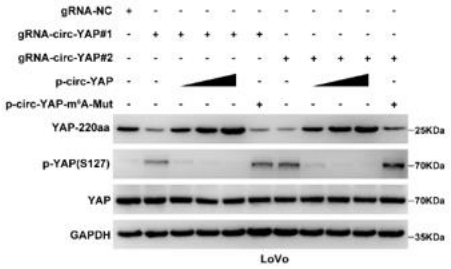

f)

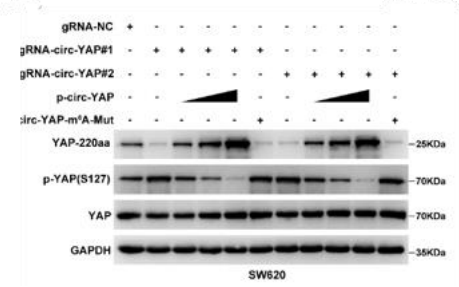

g)

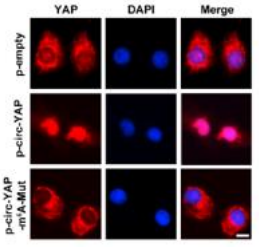

h)

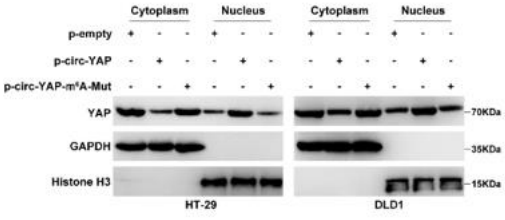

i)

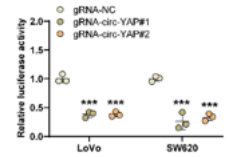

j)

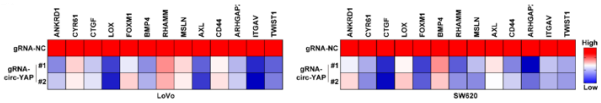

k)

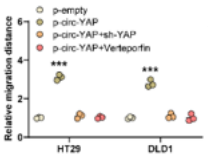

l)

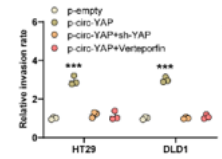

m)

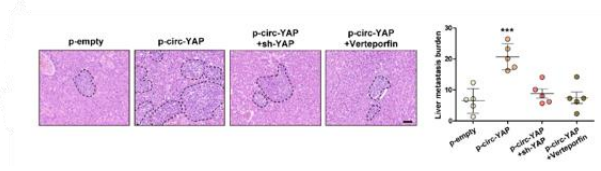

n)

Figure 5. YAP-220aa enhances YAP signaling activity. (a–c) Co-immunoprecipitation (Co-IP) assays demonstrating the interaction between YAP-220aa and LATS1.
(d, e) Co-IP analyses showing YAP association with LATS1 and 14-3-3 following circ-YAP depletion.
(f, g) Western blot analysis of the indicated proteins in circ-YAP–silenced LoVo and SW620 cells transfected with wild-type circ-YAP or m6A-mutant circ-YAP.
(h, i) Immunofluorescence staining and western blotting assessing YAP subcellular localization in circ-YAP–overexpressing cells. Scale bar, 25 μm.
(j) Luciferase reporter assay evaluating YAP transcriptional activity after circ-YAP knockdown in CRC cells.
(K) qRT-PCR analysis of YAP downstream metastasis-related gene expression following circ-YAP silencing.

(L, M) Migration and invasion assays in HT29 and DLD1 cells after YAP knockdown or verteporfin treatment.

(N) Representative images and quantification of spontaneous liver metastases in CRC models (n = 5 per group). Scale bar, 100 μm.

***P < 0.001. Data in (j, l, m) are presented as mean ± SD from three independent experiments performed in triplicate. Uncropped western blot images are provided in the Original Blot Image file.

YAP/TEAD complex transcriptionally activates circ-YAP

YAP functions as a transcriptional co-activator by interacting with transcription factors such as TEAD1–4 [21]. Notably, depletion of YAP or treatment with verteporfin markedly suppressed circ-YAP expression in both HEK293T and CRC cells **(Figure 6a)**. In contrast, expression of constitutively active YAP (YAP-5SA), but not YAP-5SA/ΔC (lacking the transactivation domain) or YAP-5SA-S94A (deficient in TEAD binding), significantly elevated circ-YAP levels. Newly synthesized circ-YAP was similarly regulated by YAP and verteporfin **(Figure 6b)**, suggesting transcriptional control.

Given that some circRNAs are transcribed from independent promoters, ChIP-seq analysis was performed and revealed strong TEAD occupancy within intron 1 of YAP pre-mRNA, a putative circ-YAP promoter region. Serial fragments of this region were cloned into a pGL3-basic reporter, and luciferase assays showed that YAP enhanced circ-YAP promoter activity within the −974 to −374 region upstream of the circ-YAP start site **(Figure 6c)**. JASPAR analysis identified two putative TEAD binding sites in this region: TB1 (−886 to −877) and TB2 (−406 to −397) **(Figure 6d)**. Mutation of either site significantly reduced promoter activity, while simultaneous mutation of both sites completely abolished YAP-5SA–induced transcriptional activation **(Figures 6e and 6f)**.

Moreover, YAP-5SA increased circ-YAP expression in TEAD2-depleted cells but failed to do so upon silencing TEAD1, TEAD3, or TEAD4; **(Figures 6g and 6h)**, indicating that TEAD1/3/4 mediate YAP-dependent circ-YAP regulation. ChIP assays further confirmed YAP binding to TB1 and TB2 **(Figure 6i)**, accompanied by recruitment and phosphorylation of RNA polymerase II **(Figures 6j and 6k)**, a key step for transcriptional elongation. ChIP-re-ChIP analyses demonstrated enrichment of the YAP/TEAD1 complex at both binding sites **(Figures 6l and 6m)**, which was further validated by DNA pull-down assays using biotin-labeled probes **(Figure 6n).**

Collectively, these findings establish circ-YAP as a direct transcriptional target of the YAP/TEAD complex, forming a positive feedback loop that facilitates CRC progression and liver metastasis.

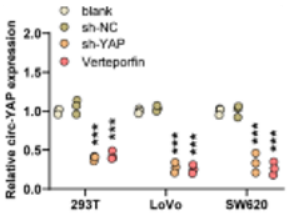

a)

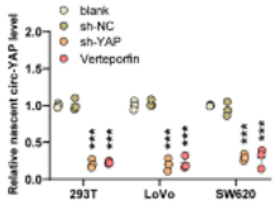

b)

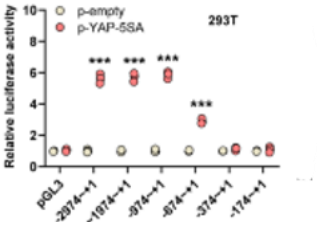

c)

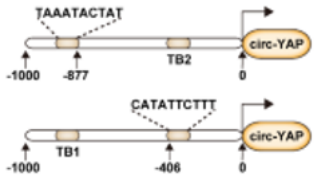

d)

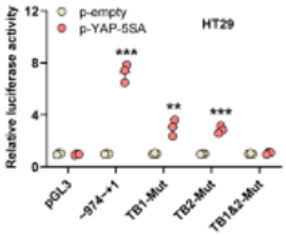

e)

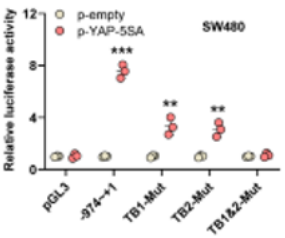

f)

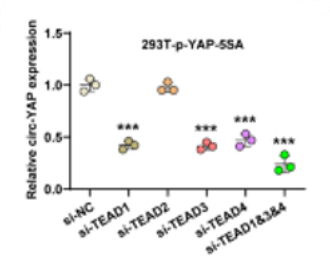

g)

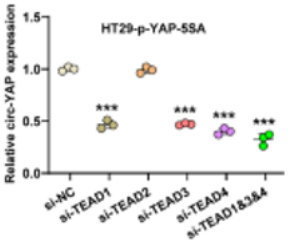

h)

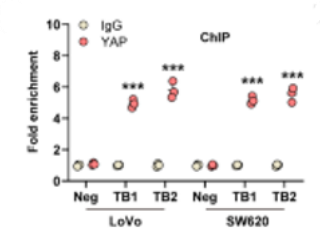

i)

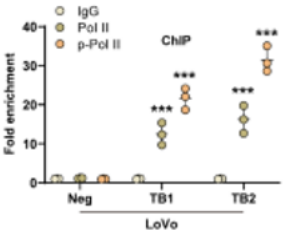

j)

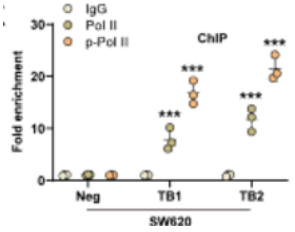

k)

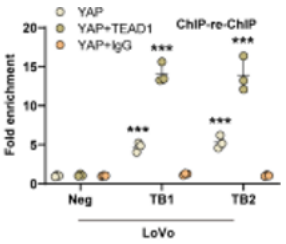

l)

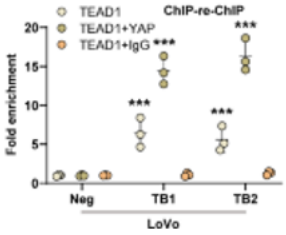

m)

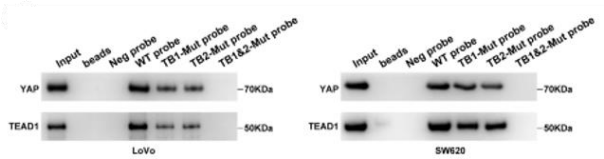

n)

Figure 6. circ-YAP is transcriptionally induced by YAP signaling**.**

(a, b) qRT-PCR quantification of total and nascent circ-YAP in cells subjected to YAP knockdown or verteporfin treatment.

(c) Luciferase reporter assays evaluating circ-YAP promoter activity in response to YAP activation.

(d) Schematic representation of two predicted YAP/TEAD binding elements within the circ-YAP promoter region.

(e, f) circ-YAP promoter activity in HT29 and SW480 cells co-transfected with constitutively active YAP (YAP-5SA) and wild-type or mutant promoter reporter constructs.

(g, h) qRT-PCR analysis of circ-YAP expression in YAP-activated cells following transfection with the indicated siRNAs.

(i–k) Chromatin immunoprecipitation (ChIP) assays using the specified antibodies, followed by qPCR to assess enrichment of YAP, RNA polymerase II (Pol II), and phosphorylated Pol II at the circ-YAP promoter.

(l, m) ChIP–re-ChIP assays with anti-YAP or anti-TEAD1 antibodies to determine co-occupancy of YAP and TEAD1 on the circ-YAP promoter.

(n) DNA pull-down assays using wild-type or mutant biotin-labeled circ-YAP promoter probes, followed by

western blot detection of YAP and TEAD1 in CRC cells.

*P < 0.05, **P < 0.01, ***P < 0.001. Data are presented as mean ± SD from three independent experiments performed in triplicate. Uncropped western blot images are provided in the Original Blot Image file

Clinical validation of the circ-YAP/YAP-220aa/YAP regulatory axis

To validate the clinical relevance of the circ-YAP/YAP-220aa/YAP signaling axis, the expression of YAP downstream target genes was examined in CRC specimens. qRT-PCR analyses revealed a positive correlation between circ-YAP levels and the expression of pro-metastatic genes, including CYR61, CTGF, TWIST1, and FOXM1 **(Figures 7a–7d)**. Immunohistochemical analyses further demonstrated concordant expression patterns of circ-YAP and YAP-220aa in 92.5% of CRC samples, with discordance observed in only 7.5% of cases **(Figures 7e and 7f)**. Elevated circ-YAP expression was also strongly associated with increased nuclear accumulation of YAP **(Figures 7e and 7g).**

Consistently, western blot analyses showed that CRC tissues with high circ-YAP expression exhibited increased levels of YAP-220aa and nuclear YAP, accompanied by reduced YAP phosphorylation. Notably, YAP-220aa expression was significantly higher in CRC patients with liver metastases than in those without metastatic disease **(Figure 7h)**. Receiver operating characteristic (ROC) analysis yielded an AUC of 0.8597 (95% CI: 0.7616–0.9125) **(Figure 7i)**, suggesting that YAP-220aa may serve as a potential biomarker for predicting CRC liver metastasis.

Importantly, patients with concurrent high expression of circ-YAP and YAP-220aa had significantly shorter overall survival compared with those exhibiting low expression of both markers **(Figure 7j)**, indicating that the combined assessment of circ-YAP and YAP-220aa provides superior prognostic value relative to circ-YAP alone **(Figure 1j).**

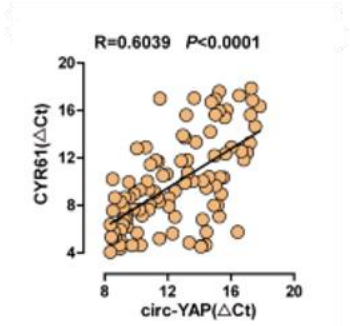

a)

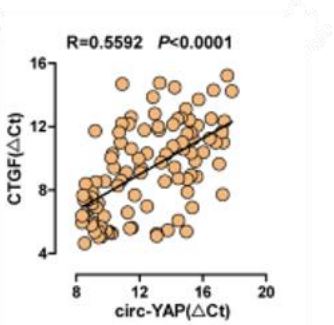

b)

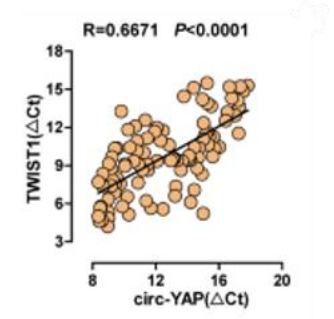

c)

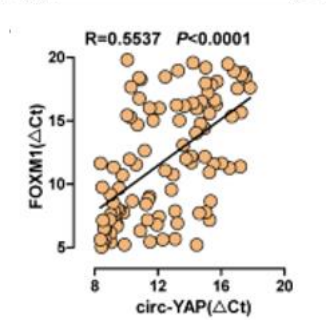

d)

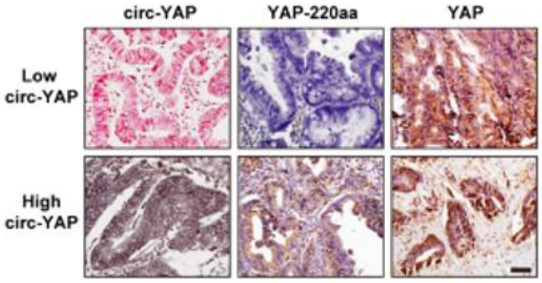

e)

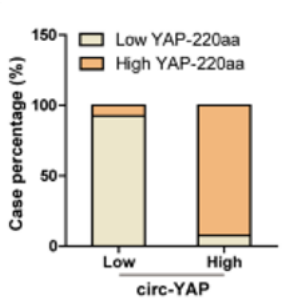

f)

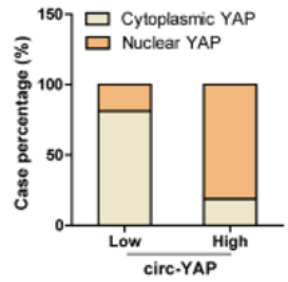

g)

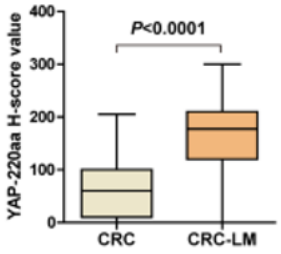

h)

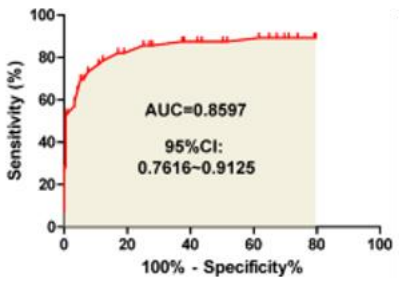

i)

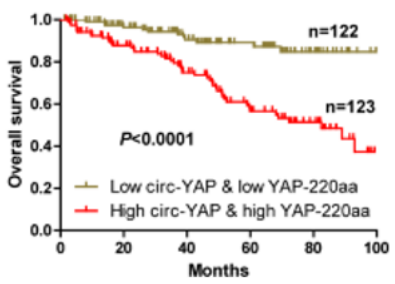

j)

Figure 7. Clinical validation of the circ-YAP/YAP-220aa/YAP signaling axis.

(a–d) Correlation analyses between circ-YAP expression and the levels of CYR61, CTGF, TWIST1, and FOXM1 in 100 colorectal cancer (CRC) specimens.

(e–g) Representative in situ hybridization (ISH) and immunohistochemistry (IHC) images showing circ-YAP, YAP-220aa, and YAP expression in CRC tissues (e), together with quantitative analyses (F, G). Scale bar, 100 μm.

(h) IHC assessment of YAP-220aa protein expression in CRC tissues with liver metastasis, followed by receiver operating characteristic (ROC) curve analysis.

(j) Kaplan–Meier survival analysis of CRC patients stratified by combined circ-YAP and YAP-220aa expression levels.

circ-YAP is translated in an m6A-dependent manner into a novel YAP isoform, YAP-220aa. The resulting YAP-220aa directly interacts with LATS1, thereby disrupting the association between LATS1 and full-length YAP. This interference reduces YAP phosphorylation, promotes its nuclear translocation, and enhances transcriptional activation of pro-metastatic genes as well as circ-YAP itself, ultimately establishing a positive feedback loop that drives CRC liver metastasis.

Circular RNAs (circRNAs) have been increasingly recognized as versatile regulators of cellular processes, acting in a context-dependent manner [22]. Their subcellular localization plays a decisive role in their function: cytoplasmic circRNAs can act as microRNA sponges, interact with diverse proteins, or serve as templates for translation into functional peptides, whereas nuclear circRNAs can influence gene transcription through interactions with DNA or transcription factors [23]. Importantly, the localization of circRNAs is dynamic and can change in response to cellular conditions, influencing disease progression [24]. For instance, circ-C9ORF72 translocates from the

nucleus to the cytoplasm under stress, contributing to neurological disorders via translation into dipeptide repeat proteins [25].

In this study, we observed that circ-YAP is predominantly cytoplasmic in both normal and CRC cells, indicating that its localization does not directly contribute to tumor initiation. Instead, circ-YAP exerts its function by being translated into a novel protein, YAP-220aa, in an m6A-dependent manner. N6-methyladenosine (m6A) is a widespread RNA modification that influences RNA metabolism, including stability, splicing, transport, and translation [26–29]. We identified a conserved "GGACA" m6A motif near the circ-YAP translation initiation site, and its mutation nearly abolished YAP-220aa production, demonstrating that a single m6A site is sufficient to drive translation. Functionally, wild-type circ-YAP, but not its m6A mutant, promoted CRC liver metastasis, underscoring the critical role of translation in circ-YAP-mediated effects. Interestingly, 7.5% of CRC samples displayed discordant levels of circ-YAP and YAP-220aa, which may reflect dysregulation of m6A machinery or translation initiation factors. Although translation requires cytoplasmic localization, a subset of circ-YAP (~20%) resides in the nucleus, suggesting additional, non-coding functions that warrant further investigation.

The Hippo-YAP pathway is a conserved regulator of organ size, cell proliferation, and differentiation, and it has emerged as a central player in tumor metastasis [20, 30, 31]. YAP activity is tightly controlled by the Hippo core kinase cascade, with LATS1-mediated phosphorylation at S127 promoting cytoplasmic retention through 14-3-3 proteins [32]. Aberrant YAP activation is commonly observed in metastatic cancers, but the mechanisms driving its dysregulation remain incompletely understood [33, 34]. Here, we identified YAP-220aa, a novel circ-YAP-encoded isoform, as a potent activator of YAP. YAP-220aa retains the WW1/2 domain essential for LATS1 binding while harboring a unique junction-spanning sequence, allowing it to competitively inhibit LATS1-mediated phosphorylation and enhance YAP nuclear translocation. Functional studies confirmed that the pro-metastatic effects of YAP-220aa require YAP activity, as knockdown of YAP or treatment with verteporfin abrogated these effects.

Mechanistically, we discovered two YAP/TEAD binding motifs upstream of circ-YAP, and mutation of these sites completely abolished YAP-mediated transcriptional activation of circ-YAP, revealing a previously unrecognized positive feedback loop that amplifies circ-YAP-driven CRC liver metastasis. Given the challenges of directly targeting YAP as a transcriptional co-activator, modulating regulators such as YAP-220aa may represent a more feasible therapeutic strategy [35]. Collectively, our findings establish circ-YAP and its translation product YAP-220aa as key drivers of Hippo-YAP pathway activation in CRC and highlight their potential as prognostic biomarkers and targets for intervention.

Limitations

This study has several limitations. The primary concern is that our in vitro and in vivo experiments relied on conventional 2D human cell lines, which do not fully capture the heterogeneity, clonal diversity, and complex growth patterns of clinical tumors. Incorporating advanced 3D organoid models could provide a more physiologically relevant platform to validate our findings. Additionally, our analyses were based on retrospectively collected patient samples, which may introduce biases due to differences in prior treatments and clinical management.

Conclusion

In summary, our work reveals a previously unrecognized link between a circRNA-encoded protein and Hippo/YAP signaling, highlighting a novel mechanism that drives CRC liver metastasis. These findings provide valuable insights for the development of prognostic biomarkers and potential therapeutic strategies targeting this pathway.

Acknowledgments: None

Conflict of Interest: None

Financial Support: This study was supported by grants from the National Natural Science Foundation of China (82303440, 82103273 and 82203626), Natural Science Basic Research Program of Shaanxi Province (2022JQ-825), Shaanxi Provincial Health Research Fund (2022E022), Project funded by China Postdoctoral Science Foundation (2021M700108, 2022T150520), the Guangdong Basic and Applied Basic Research Foundation (2023A1515010523, 2023A1515010473, 2021A1515110509, and 2019A1515110144), the Medical Scientific Research Foundation of Guangdong

Province (A2021130), Fundamental Research Funds for the Central Universities (xzy012021063) and Free Exploration and Innovation Fund (2020YJ(ZYTS)546 − 12).

Ethics Statement: This study was approved by the Institutional Ethical Review Boards of Sun Yat-sen University Cancer Center (SL-B2022-276-02). Informed consent was obtained from the participated patients. All procedures for animal experiments were approved by the Institutional Animal Care and Use Committee of Sun Yat-sen University (SYSU-IACUC-2021-000653).

References

1. Sung H, Ferlay J, Siegel RL, et al. Global Cancer Statistics 2020: GLOBOCAN estimates of incidence and Mortality Worldwide for 36 cancers in 185 countries. CA Cancer J Clin. 2021;71:209–49. doi: 10.3322/caac.21660
2. Osei-Bordom DC, Kamarajah S, Christou N. Colorectal Cancer, Liver Metastases and Biotherapies. Biomedicines. 2021, 9.
3. Tsilimigras DI, Brodt P, Clavien PA, et al. Liver metastases. Nat Rev Dis Primers. 2021;7:27. doi: 10.1038/s41572-021-00261-6
4. Patop IL, Wust S, Kadener S. Past, present, and future of circRNAs. EMBO J. 2019;38:e100836. doi: 10.15252/embj.2018100836
5. Kristensen LS, Andersen MS, Stagsted L, Ebbesen KK, Hansen TB, Kjems J. The biogenesis, biology and characterization of circular RNAs. Nat Rev Genet. 2019;20:675–91. doi: 10.1038/s41576-019-0158-7
6. Chen X, Zhou M, Yant L, Huang C. Circular RNA in disease: Basic properties and biomedical relevance. Wiley Interdiscip Rev RNA. 2022;13:e1723. doi: 10.1002/wrna.1723
7. Lei M, Zheng G, Ning Q, Zheng J, Dong D. Translation and functional roles of circular RNAs in human cancer. Mol Cancer. 2020;19:30. doi: 10.1186/s12943-020-1135-7
8. Kristensen LS, Jakobsen T, Hager H, Kjems J. The emerging roles of circRNAs in cancer and oncology. Nat Rev Clin Oncol. 2022;19:188–206. doi: 10.1038/s41571-021-00585-y
9. Memczak S, Jens M, Elefsinioti A, et al. Circular RNAs are a large class of animal RNAs with regulatory potency. Nature. 2013;495:333–8. doi: 10.1038/nature11928
10. Hansen TB, Jensen TI, Clausen BH, et al. Natural RNA circles function as efficient microRNA sponges. Nature. 2013;495:384–8. doi: 10.1038/nature11993
11. Huang A, Zheng H, Wu Z, Chen M, Huang Y. Circular RNA-protein interactions: functions, mechanisms, and identification. Theranostics. 2020;10:3503–17. doi: 10.7150/thno.42174
12. Du WW, Xu J, Yang W, et al. A neuroligin isoform translated by circNlgn contributes to Cardiac Remodeling. Circ Res. 2021;129:568–82. doi: 10.1161/CIRCRESAHA.120.318364
13. Gao X, Xia X, Li F, et al. Circular RNA-encoded oncogenic E-cadherin variant promotes glioblastoma tumorigenicity through activation of EGFR-STAT3 signalling. Nat Cell Biol. 2021;23:278–91. doi: 10.1038/s41556-021-00639-4
14. Li Y, Chen B, Zhao J, et al. HNRNPL Circularizes ARHGAP35 to produce an oncogenic protein. Adv Sci (Weinh) 2021;8:2001701. doi: 10.1002/advs.202001701
15. Wen SY, Qadir J, Yang BB. Circular RNA translation: novel protein isoforms and clinical significance. Trends Mol Med. 2022;28:405–20. doi: 10.1016/j.molmed.2022.03.003
16. Jiang X, Liu B, Nie Z, et al. The role of m6A modification in the biological functions and diseases. Signal Transduct Target Ther. 2021;6:74. doi: 10.1038/s41392-020-00450-x
17. Zeng K, Chen X, Hu X, et al. LACTB, a novel epigenetic silenced tumor suppressor, inhibits colorectal cancer progression by attenuating MDM2-mediated p53 ubiquitination and degradation. Oncogene. 2018;37:5534–51. doi: 10.1038/s41388-018-0352-7
18. Li S, Li X, Xue W, et al. Screening for functional circular RNAs using the CRISPR-Cas13 system. Nat Methods. 2021;18:51–9. doi: 10.1038/s41592-020-01011-4
19. Yang Y, Fan X, Mao M, et al. Extensive translation of circular RNAs driven by N(6)-methyladenosine. Cell Res. 2017;27:626–41. doi: 10.1038/cr.2017.31
20. Moya IM, Halder G. Hippo-YAP/TAZ signalling in organ regeneration and regenerative medicine.

Nat Rev Mol Cell Biol. 2019;20:211–26. doi: 10.1038/s41580-018-0086-y.

21. Ibar C, Irvine KD. Integration of Hippo-YAP signaling with metabolism. Dev Cell. 2020;54:256–67. doi: 10.1016/j.devcel.2020.06.025
22. Plawgo K, Raczynska KD. Context-dependent regulation of Gene expression by Non-Canonical Small RNAs. Noncoding RNA. 2022, 8.
23. Misir S, Wu N, Yang BB. Specific expression and functions of circular RNAs. Cell Death Differ. 2022;29:481–91. doi: 10.1038/s41418-022-00948-7
24. Yang Q, Li F, He AT, Yang BB. Circular RNAs: expression, localization, and therapeutic potentials. Mol Ther. 2021;29:1683–702. doi: 10.1016/j.ymthe.2021.01.018
25. Wang S, Latallo MJ, Zhang Z, et al. Nuclear export and translation of circular repeat-containing intronic RNA in C9ORF72-ALS/FTD. Nat Commun. 2021;12:4908. doi: 10.1038/s41467-021-25082-9
26. Deng LJ, Deng WQ, Fan SR, et al. m6A modification: recent advances, anticancer targeted drug discovery and beyond. Mol Cancer. 2022;21:52. doi: 10.1186/s12943-022-01510-2
27. Zhang F, Liu H, Duan M, et al. Crosstalk among m(6)a RNA methylation, hypoxia and metabolic reprogramming in TME: from immunosuppressive microenvironment to clinical application. J Hematol Oncol. 2022;15:84. doi: 10.1186/s13045-022-01304-5
28. Frye M, Harada BT, Behm M, He C. RNA modifications modulate gene expression during development. Science. 2018;361:1346–9. doi: 10.1126/science.aau1646
29. Niu X, Yang Y, Ren Y, Zhou S, Mao Q, Wang Y. Crosstalk between m(6)a regulators and mRNA during cancer progression. Oncogene. 2022.
30. Li HL, Li QY, Jin MJ, et al. A review: hippo signaling pathway promotes tumor invasion and metastasis by regulating target gene expression. J Cancer Res Clin Oncol. 2021;147:1569–85. doi: 10.1007/s00432-021-03604-8
31. Zanconato F, Cordenonsi M, Piccolo S. YAP and TAZ: a signalling hub of the tumour microenvironment. Nat Rev Cancer. 2019;19:454–64. doi: 10.1038/s41568-019-0168-y
32. Zhao B, Li L, Tumaneng K, Wang CY, Guan KL. A coordinated phosphorylation by lats and CK1 regulates YAP stability through SCF(beta-TRCP) Genes Dev. 2010;24:72–85. doi: 10.1101/gad.1843810
33. Warren J, Xiao Y, Lamar JM. YAP/TAZ activation as a target for treating Metastatic Cancer. Cancers (Basel). 2018. 10.
34. Tocci P, Blandino G, Bagnato A. YAP and endothelin-1 signaling: an emerging alliance in cancer. J Exp Clin Cancer Res. 2021;40:27. doi: 10.1186/s13046-021-01827-8
35. Yan F, Qian M, He Q, Zhu H, Yang B. The posttranslational modifications of Hippo-YAP pathway in cancer. Biochim Biophys Acta Gen Subj. 2020;1864:129397. doi: 10.1016/j.bbagen.2019.07.006